

Mn²⁺ Sites in the Hammerhead Ribozyme Investigated by EPR and Continuous-Wave Q-band ENDOR Spectroscopies

Susan R. Morrissey, Thomas E. Horton, and Victoria J. DeRose*

Contribution from the Department of Chemistry, Texas A&M University,
College Station, Texas 77842-3012

Received August 17, 1999. Revised Manuscript Received January 21, 2000

Abstract: Metal ions are critical to the structure and function of many RNA molecules, but measuring detailed coordination environments in RNA is challenging under solution conditions. The phosphodiester bond cleavage reaction of the hammerhead ribozyme is activated by Mn²⁺, which provides a paramagnetic probe for EPR-based spectroscopic techniques. In this study, EPR and continuous-wave Q-band (34 GHz) electron nuclear double-resonance (ENDOR) spectroscopies have been used to investigate the coordination environment of a high-affinity Mn²⁺ site in the hammerhead ribozyme. Small changes in low-temperature X-band EPR signals are detected as signatures of Mn²⁺ ions in the RNA binding pocket. ¹H and ³¹P Q-band ENDOR spectra are presented for Mn–hammerhead and Mn–nucleotide model complexes. The ³¹P ENDOR data allow discrimination between direct Mn²⁺–phosphodiester coordination versus coordination through a hydrogen-bonded water molecule. Observation of hyperfine-coupled ³¹P (*A*(³¹P) ~4 MHz) provides evidence for direct coordination to a phosphodiester group in the hammerhead Mn²⁺ site. Exchangeable protons from aqueous ligands and nonexchangeable protons from base ligands also are examined for the Mn–nucleotide and Mn–ribozyme complexes. These signals indicate an ordered site for Mn²⁺ in the hammerhead ribozyme and allow the ligand environment to be predicted, demonstrating the potential of ENDOR spectroscopy as a probe of RNA–metal interactions.

Introduction

Protein-catalyzed phosphoryl transfer reactions are critical in many biological processes, including nucleic acid synthesis and degradation as well as nucleotide-dependent signaling events. Many enzymes performing this class of reactions contain active-site divalent metal ions, predominantly Zn²⁺, Mg²⁺, or Mn²⁺, whose roles in catalysis have long been an active area of research.^{1,2} Naturally occurring chemically active RNA molecules (“ribozymes”) also perform metal-activated phosphoryl-transfer reactions during their activities in RNA self-processing reactions.^{3,4} Roles for metal cofactors in RNA-catalyzed reactions are not yet understood, but are expected to be expanded from those in proteins to include stabilization of RNA tertiary structure as well as participation in the chemical reaction.

An obstacle to investigating roles of metal ions in RNA catalysis has been the challenge of obtaining precise metal–RNA structural information under solution conditions. In protein

systems, EPR and related spectroscopies have been highly informative for the many cases in which Mn²⁺ supports activity.^{5–12} Mn²⁺ EPR signals reflect ligand-induced zero field splitting parameters, but the EPR line widths often are too broad to directly observe hyperfine interactions to ligand nuclei. Electron nuclear double-resonance (ENDOR) and electron spin–echo envelope modulation (ESEEM) spectroscopic techniques can provide metal–ligand identification and geometries through direct measurement of electron–nuclear hyperfine interactions.¹³ In the case of phosphoryl-transfer reactions, nuclei such as ¹H

(5) Reed, G. H.; Markham, G. D. *Biol. Magn. Reson.* **1984**, *6*, 73–142.

(6) McCracken, J.; Peisach, J.; Bhattacharyya, L.; Brewer, F. *Biochemistry* **1991**, *30*, 4486–4491.

(7) (a) Larsen, R. G.; Halkides, C. J.; Redfield, A. G.; Singel, D. J. *J. Am. Chem. Soc.* **1992**, *114*, 9608–9611. (b) Halkides, C. J.; Farrar, C. T.; Larsen, R. G.; Redfield, A. G.; Singel, D. J. *Biochemistry* **1994**, *33*, 4019–4035. (c) Halkides, C. J.; Bellew, B. F.; Gerfen, G. J.; Farrar, C. T.; Carter, P. H.; Ruo, B.; Evans, D. A.; Griffin, R. G.; Singel, D. J. *Biochemistry* **1996**, *35*, 12194–12200.

(8) Espe, M. P.; Hosler, J. P.; Ferguson-Miller, S.; Babcock, G. T.; McCracken, J. *Biochemistry* **1995**, *34*, 7593–7602.

(9) LoBrutto, R.; Smithers, G. W.; Reed, G. H.; Orme-Johnson, W. H.; Tan, S. L.; Leigh, J. S., Jr. *Biochemistry* **1986**, *25*, 5654–5660.

(10) (a) Serpersu, E. H.; McCracken, J.; Peisach, J.; Mildvan, A. S. *Biochemistry* **1988**, *27*, 8034–8044. (b) Tipton, P. A.; McCracken, J.; Cornelius, J. B.; Peisach, J. *Biochemistry* **1989**, *28*, 5720–5728.

(11) Buy, C.; Girault, G.; Zimmermann, J.-L. *Biochemistry* **1996**, *35*, 9880–9891.

(12) Tan, X.; Poyner, R.; Reed, G. H.; Scholes, C. P. *Biochemistry* **1993**, *32*, 7799–7810.

(13) (a) Hoffman, B. M.; DeRose, V. J.; Doan, P. E.; Gurbel, R. J.; Houseman, A. L. P.; Telsler, J. *Biol. Magn. Reson.* **1993**, *13*, 151–218. (b) DeRose, V. J.; Hoffman, B. M. *Methods Enzymol.* **1995**, *246*, 554–589. (c) Britt, R. D. In *Advances in Photosynthesis: Biophysical Techniques in Photosynthesis*; Hoff, A. J., Ames, J., Eds.; Kluwer Academic Publishers: Amsterdam, 1995; pp 235–253. (d) Mims, W. B.; Peisach, J. In *Biological Magnetic Resonance*; Berliner, L. J., Ruben, J., Eds.; Plenum Press: New York, 1981; pp 213–263.

* Corresponding author. Phone: 979-862-1401. Fax: 979-845-4719. email: derose@mail.chem.tamu.edu.

(1) Lipscomb, W. N.; Sträter, N. *Chem. Rev.* **1996**, *96*, 2375–2433.

(2) Wilcox, D. E. *Chem. Rev.* **1996**, *96*, 2435–2458.

(3) Abbreviations: RNA, ribonucleic acid; DNA, deoxyribonucleic acid; GMP, guanosine monophosphate; ATP, adenosine triphosphate; NMR, nuclear magnetic resonance; EPR, electron paramagnetic resonance; ENDOR, electron nuclear double resonance; ESEEM, electron spin–echo envelope modulation; CW, continuous wave; rf, radio frequency; ptp, peak to peak; i.d., inner diameter; o.d., outer diameter; nt, nucleotide; zfs, zero field splitting.

(4) (a) Cech, T. R. In *The RNA World*; Gesteland, R., Atkins, J., Eds.; Cold Spring Harbor Laboratory Press: Cold Spring Harbor, NY, 1993; pp 239–270. (b) Pan, T.; Long, D. M.; Uhlenbeck, O. C. In *The RNA World*; Gesteland, R., Atkins, J., Eds.; Cold Spring Harbor Laboratory Press: Cold Spring Harbor, NY, 1993; pp 271–302. (c) Pyle, A. M. *Science* **1993**, *261*, 709–714. (d) Narlikar, G. J.; Herschlag, D. *Annu. Rev. Biochem.* **1997**, *66*, 19–59.

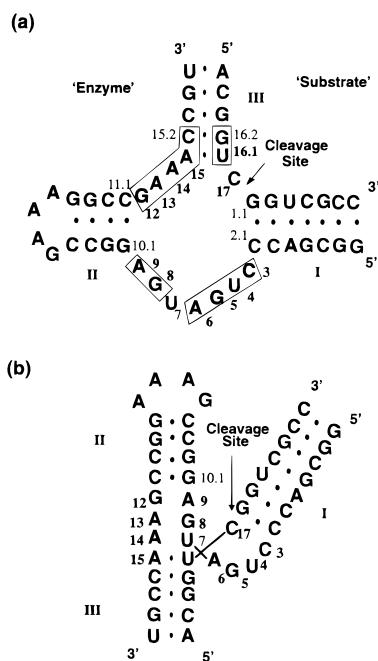


Figure 1. Hammerhead sequence used in this study.^{39a} The construct consists of an “enzyme” and a “substrate” strand hybridized via complementary arms I and III. An arrow marks the cleavage site on the substrate strand. The 13-nt conserved core is enclosed in the boxes. To prevent phosphodiester bond cleavage, a DNA “substrate” strand was used for spectroscopic studies. (b) Schematic of the tertiary structure of the ribozyme based on crystallographic models.

(both exchangeable and nonexchangeable), ^{14/15}N, ¹³C, and ³¹P are potential structural probes near to the active-site metal ion.

In this work, we use Q-band (34 GHz) CW ENDOR spectroscopy to analyze ligand hyperfine interactions for a Mn²⁺ site in a structured RNA molecule, the hammerhead ribozyme. Metal–RNA ligand environments, not previously explored using ENDOR, are expected to exhibit contributions from phosphodiester, base, and aqueous ligands whose hyperfine couplings can be compared with those previously observed in Mn²⁺–phosphate and –protein environments.

The hammerhead ribozyme is a small RNA molecule that cleaves a specific phosphodiester bond, in a reaction highly activated by divalent metal ions.^{4,14–17} The hammerhead is commonly constructed as an “enzyme” strand that targets and cleaves a “substrate” ribooligonucleotide (Figure 1). The complementary arms of the hammerhead and other ribozymes can be altered to target essentially any RNA sequence, and so ribozymes are very specific RNA-cleavage agents that have potential as gene therapeutic agents.¹⁸

(14) (a) Hutchins, C. J.; Rathjen, P. D.; Forster, A. C.; Symons, R. H. *Nucleic Acids Res.* **1986**, *14*, 3627–3640. (b) Uhlenbeck, O. C. *Nature* **1987**, *328*, 596–600.

(15) Reviewed in: (a) Bratty, J.; Chartrand, P.; Ferbeyre, G.; Cedergren, R. *Bioch. Biophys. Acta* **1993**, *1216*, 345–359. (b) McKay, D. B. *RNA* **1996**, *2*, 395–403. (c) Wedekind, J. E.; McKay, D. B. *Annu. Rev. Biophys. Biomol. Struct.* **1998**, *27*, 475–502.

(16) (a) Dahm, S. C.; Derrick, W. B.; Uhlenbeck, O. C. *Biochemistry* **1993**, *32*, 13040–13045. (b) Dahm, S. C.; Uhlenbeck, O. C. *Biochemistry* **1991**, *30*, 9464–9469. (c) Lott, W. B.; Pontius, B. W.; von Hippel, P. H. *Proc. Natl. Acad. Sci. U.S.A.* **1998**, *95*, 542–547. (d) Zhou, D.-M.; Kumar, P. K. R.; Zhang, L.-H.; Taira, K. *J. Am. Chem. Soc.* **1996**, *118*, 8969–8970. (e) Zhou, D.-M.; He, Q.-C.; Zhou, J.-M.; Taira, K. *FEBS Lett.* **1998**, *431*, 154–160.

(17) Horton, T. E.; Clardy, D. R.; DeRose, V. J. *Biochemistry* **1998**, *37*, 18094–18101.

(18) (a) James, H. A.; Gibson, I. *Blood* **1998**, *91*, 371–382. (b) Bramlage, B.; Alefelder, S.; Marschall, P.; Eckstein, F. *Nucleic Acids Res.* **1999**, *27*, 3159–3167.

Several roles have been suggested for metal ions in the chemical step of hammerhead phosphodiesterase activity.^{4,15,16} The hammerhead ribozyme reaction is an S_N2-type transesterification wherein the cleavage site sugar 2'-OH acts as a nucleophile on its 3'-phosphodiester bond, yielding 2',3'-cyclic phosphate and 5'-OH terminated products. Proposed roles for metal ions in this reaction include activating the 2'-OH nucleophile, possibly through deprotonation by the metal hydroxide species, and/or coordinating to the phosphodiester substrate. Mechanisms invoking either one or two metal ions to fulfill these roles have been proposed for the hammerhead and other ribozymes.^{15,16,19}

Divalent cations in specific binding pockets also may stabilize tertiary structures critical for RNA activity.²⁰ Consistent with this, metal-dependent structural transitions have been reported for the hammerhead ribozyme.^{21,22} In addition, metal-dependent activity is altered by substitutions at sites that, based on X-ray crystallographic models, are predicted to be many angstroms distant from the hammerhead cleavage site.^{15,23,24} Both of these results are consistent with metal sites whose role may be to stabilize an active tertiary structure.

In an effort to quantitatively understand the metal ions required for the hammerhead reaction, we previously examined global Mn²⁺–hammerhead binding properties and their relationship to activity.¹⁷ In 100 mM NaCl, the hammerhead sequence of Figure 1 has four high-affinity or “tight” Mn²⁺ sites ($K_d \sim 4 \mu\text{M}$) and a second class of weaker sites ($K_d \sim 400 \mu\text{M}$). By contrast, in 1 M NaCl a single “tight” site ($K_d \sim 10 \mu\text{M}$) in the hammerhead is populated at low Mn²⁺ concentrations, and the remaining sites are occupied at higher concentrations of Mn²⁺ following an apparent cooperative transition. In both 0.1 and 1.0 M NaCl, there is a lag in hammerhead activity before the high-affinity Mn²⁺ sites are filled, and in fact, maximal activity is not reached until beyond Mn²⁺ concentrations required to populate both types of sites. The high-affinity Mn²⁺ sites are abolished by mutations in the conserved core of the hammerhead,²⁵ and in particular by the A14-G mutation that is also proposed to inhibit folding of the RNA.²² Thus, the activity lag at low Mn²⁺ concentrations may be due to metal-dependent conformational changes in the RNA tertiary structure that are required for activity.

The current goal is to use spectroscopic techniques to examine the ligand environments of the high-affinity Mn²⁺ sites in the hammerhead ribozyme. Previous X-band Mn²⁺ EPR, ENDOR, and ESEEM studies of protein systems lay the groundwork for spectroscopic studies in this area. Tan et al.²⁶ fully analyzed the ¹H ENDOR spectra from Mn(H₂O)₆²⁺ and examined a Mn²⁺–oxalate–ATP complex in pyruvate kinase.¹² Hyperfine

(19) Steitz, T. A.; Steitz, J. A. *Proc. Natl. Acad. Sci. U.S.A.* **1993**, *90*, 6498–6502.

(20) Reviewed in: Misra, V. K.; Draper, D. E. *Biopolymers* **1998**, *48*, 113–135.

(21) Menger, M.; Tuschl, T.; Eckstein, F.; Porschke, D. *Biochemistry* **1996**, *35*, 14710–14716.

(22) (a) Bassi, G. S.; Millegaard, N. E.; Murchie, A. I. H.; Lilley, D. M. J. *Biochemistry* **1999**, *38*, 3345–3354. (b) Bassi, G. S.; Murchie, A. I. H.; Lilley, D. M. J. *RNA* **1996**, *2*, 756–768. (c) Bassi, G. S.; Murchie, A. I. H.; Walter, F.; Clegg, R. M.; Lilley, D. M. J. *EMBO J.* **1997**, *16*, 7481–7489.

(23) (a) Ruffner, D. E.; Uhlenbeck, O. C. *Nucleic Acids Res.* **1990**, *18*, 6025–6029. (b) Peracchi, A.; Beigelman, L.; Scott, E. C.; Uhlenbeck, O. C.; Herschlag, D. *J. Biol. Chem.* **1997**, *272*, 26822–26826. (c) Knöll, R.; Bald, R.; Fürste, J. P. *RNA*, **1997**, 132–140.

(24) Peracchi, A.; Beigelman, L.; Usman, N.; Herschlag, D. *Proc. Natl. Acad. Sci. U.S.A.* **1996**, *93*, 11522–11527.

(25) Hunsicker, L. M.; DeRose, V. J., in preparation.

(26) Tan, X.; Bernardo, M.; Thomann, H.; Scholes, C. P. *J. Chem. Phys.* **1993**, *98*, 5147–5157.

couplings to ³¹P in ATP and ¹⁷O in ATP and oxalate were reported from this protein study. These and other studies²⁷ have reported ENDOR features from the $|m_s| > 1/2$ sublevels in the Mn²⁺ $S = 5/2$ EPR spectrum. The separations of these features can be amplified by up to 5 times those observed from within the $|m_s| = \pm 1/2$ sublevels, and in favorable cases, this property may lead to enhanced resolution of small hyperfine couplings.

In this study, the X- and Q-band frozen solution EPR spectra of Mn²⁺ bound in the high-affinity sites of the hammerhead ribozyme are explored. Small changes in the EPR signals are detected as signatures of Mn²⁺ ions in the RNA binding pocket. ¹H and ³¹P Q-band ENDOR spectra are presented for Mn–hammerhead and Mn–nucleotide model complexes. The ³¹P ENDOR data allow discrimination between direct Mn²⁺–phosphodiester coordination versus coordination through a hydrogen-bonded water molecule. Exchangeable protons from aqueous ligands and nonexchangeable protons from base ligands also are examined. These signals indicate an ordered site for Mn²⁺ in the hammerhead ribozyme and allow the ligand environment to be predicted, demonstrating the potential of ENDOR spectroscopy as a probe of RNA–metal interactions.

Results

EPR and ENDOR data were obtained for a hammerhead ribozyme sample poised in 1 M NaCl and at a ratio of 1:1 Mn²⁺ to ribozyme. Under these conditions, a single high-affinity Mn²⁺ site is populated.¹⁷ To understand the ENDOR features expected for different Mn²⁺–¹H and Mn²⁺–³¹P distances, spectra also were obtained for Mn(H₂O)₆²⁺ and for two Mn–nucleotide complexes, Mn–GMP and Mn–ATP. The latter samples were prepared in a 1:10 Mn²⁺:nucleotide ratio to ensure full metal ion complexation. In Mn–GMP, the Mn²⁺ ion is expected to be directly coordinated to the N7 position of the guanine base and coordinated in an outer-sphere manner through a water molecule to the 5′-monophosphate.²⁸ By contrast, when complexed to ATP, Mn²⁺ is directly coordinated to at least two of the phosphodiester groups and may be coordinated to the adenine N7 position²⁹ (this point is considered in further detail below).

EPR. In Figure 2 the low-temperature X-band EPR spectra of Mn(H₂O)₆²⁺, Mn–ATP, and Mn–ribozyme complexes are compared. The Mn²⁺ $S = 5/2$, $I = 5/2$ EPR signal arises from sets of allowed $\Delta m_s = \pm 1$, $\Delta m_l = 0$ transitions. In frozen solution and in the presence of small ligand asymmetries that give rise to nonzero zero-field splitting terms, the features that arise from these transitions are separated into the familiar six-line pattern from the $m_s = \pm 1/2$ manifold and broader, unresolved “wings” due to transitions involving the higher m_s manifolds. Between the six main peaks in the EPR spectrum, small features appear that arise predominately from semiforbidden $\Delta m_l = \pm 1$ features that depend on second- and third-order effects involving the zero field splitting (zfs) terms.⁵

(27) (a) Sturgeon, B. E.; Ball, J. A.; Randall, D. W.; Britt, R. D. *J. Phys. Chem.* **1994**, *98*, 12871–12883. (b) Arieli, D.; Vaughan, D. E. W.; Strohmaier, K. G.; Goldfarb, D. *J. Am. Chem. Soc.* **1999**, *121*, 6028–6032.

(28) (a) De Meester, P.; Goodgame, D. M. L.; Jones, T. J.; Skapski, A. C. *Biochem. J.* **1974**, *139*, 791–792. (b) Tajmir-Riahi, H. A.; Theophanides, T. *Can. J. Chem.* **1983**, *61*, 1813–1822.

(29) (a) Sternlicht, H.; Shulman, R. G.; Anderson, E. W. *J. Chem. Phys.* **1965**, *43*, 3133–3143. (b) Sternlicht, H.; Jones, D. E.; Kustin, K. *J. Am. Chem. Soc.* **1968**, *90*, 7110–7118. (c) Glassman, T. A.; Cooper, C.; Harrison, L. W.; Swift, T. J. *Biochemistry* **1971**, *10*, 843–851. (d) Wee, V.; Feldman, I.; Rose, P.; Gross, S. *J. Am. Chem. Soc.* **1974**, *96*, 103–112. (e) Sabat, M.; Cini, R.; Haromy, T.; Sundaralingam, M. *Biochemistry* **1985**, *24*, 7827–7833. (f) Sigel, H.; Tribolet, R.; Malini-Balakrishnan, R.; Martin, R. B. *Inorg. Chem.* **1987**, *26*, 2149–2157. (g) Sigel, H. *Eur. J. Biochem.* **1987**, *165*, 65–72.

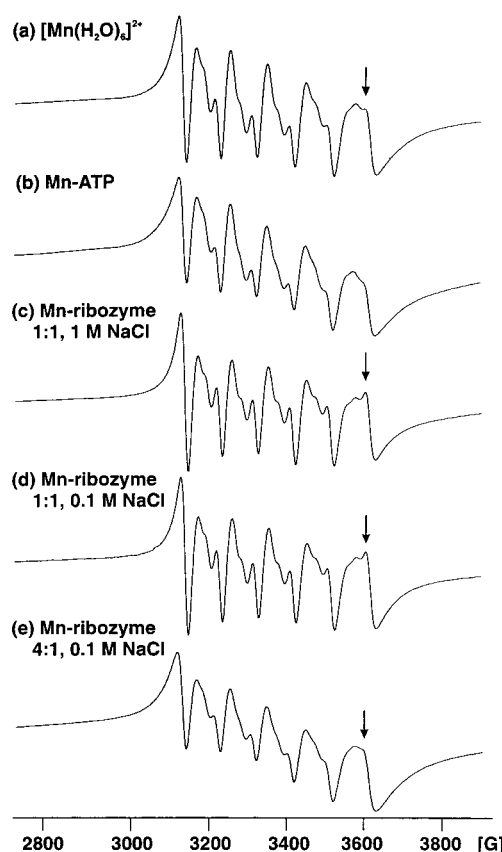


Figure 2. Low-temperature X-band EPR spectra of (a) Mn(H₂O)₆²⁺, (b) 1 mM Mn and 10 mM ATP, (c) 1 mM Mn and 1 mM ribozyme in 1 M NaCl, (d) 1 mM Mn and 1 mM ribozyme in 100 mM NaCl, and (e) 1 mM Mn and 250 μ M ribozyme in 100 mM NaCl. Arrows indicate features that are altered in 1:1 Mn/ribozyme complexes. EPR parameters: 10 K, 15 G ptp field modulation, 0.063 mW microwave power, 9.44 GHz, and 1 scan.

Changes due to different Mn²⁺ ligand environments can be detected from the details of these EPR features.

The low-temperature X-band EPR spectrum of a 1:1 Mn–ribozyme complex in 1 M NaCl is similar to that of Mn(H₂O)₆²⁺ in the same buffer, except for a subtle and reproducible alteration in structure between the fifth and sixth Mn²⁺ hyperfine lines (arrows in Figures 2). This small difference provides an EPR signature for the Mn²⁺ in the ribozyme site. The same feature is observed in a 1:1 Mn–ribozyme sample in 0.1 M NaCl (Figure 2d), indicating that the highest-affinity site is likely identical in both NaCl conditions.

In 0.1 M NaCl, the ribozyme has four high-affinity Mn²⁺ sites. Additional equivalents of Mn²⁺ added to the ribozyme in 0.1 M NaCl cause broadening and loss of the signature feature in the X-band EPR signal (Figure 2e), as well as an increase in the average microwave power saturation parameter $P_{1/2}$ (data not shown). Of note, no signals were observed that would indicate a dinuclear [Mn(II)]₂ site in these samples (see Discussion).

The Q-band EPR spectra shown in Figure 3 are detected in dispersion mode under rapid passage conditions and so appear as absorption line shapes. The main contributions to the central six-line pattern are from the $m_s = 1/2 \leftrightarrow -1/2$ transitions.⁵ Lying under the central pattern are broad, unresolved contributions from the higher m_s states, which extend into the wings of the spectrum.^{5,26,27} In the experimental spectra, the $\Delta m_s = \pm 1$ transitions from the $\pm 1/2 \leftrightarrow \pm 3/2$ and $\pm 3/2 \leftrightarrow \pm 5/2$ m_s levels do not show resolved ⁵⁵Mn hyperfine couplings because of increas-

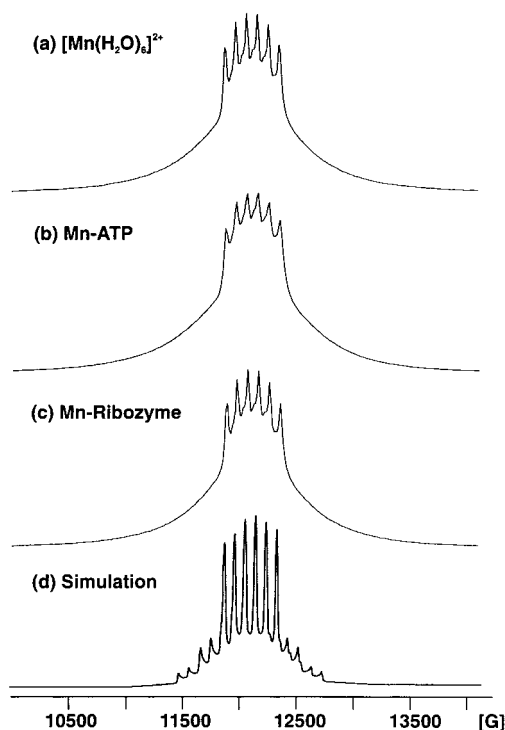


Figure 3. Dispersion-detected Q-band EPR spectra of (a) $\text{Mn}(\text{H}_2\text{O})_6^{2+}$, (b) Mn-ATP, and (c) Mn-ribozyme. All samples are 1 mM Mn^{2+} and 1.0 M NaCl. (d) Simulation using the following parameters: $g = 2.00$, $A(^{55}\text{Mn}) = 91$ G; $D = -200$ G; line width 10 G, 33.90 GHz microwave frequency. EPR parameters: 2.0 K, 1.7 mW, 0.5 G ptp field modulation, and 1 scan. (a) 33.90, (b) 33.89, and (c) 33.92 GHz.

ing zfs-dependent line broadening. The simulation in Figure 3d uses a value of $D = -200$ G, similar to values used in previous X-band EPR spectral simulations of $\text{Mn}(\text{H}_2\text{O})_6^{2+}$,²⁶ which approximately matches the breadth of the Mn-ribozyme spectrum. The EPR simulation program used for the simulation in Figure 3d does not include an m_s -specific line width,³⁰ and so the wings of the spectrum exhibit resolved ^{55}Mn splittings.

^1H ENDOR. ENDOR obtained at any position on the Mn^{2+} EPR signal will be a superposition of signals from all $\Delta m_s = \pm 1$ transitions of the $S = 5/2$ Mn^{2+} ion that contribute at that magnetic field position. Hyperfine splittings from the $m_s = +3/2$ and $\pm 5/2$ sublevels are multiplied by factors of 3 and 5, respectively, over those observed for the EPR transitions between the $m_s = \pm 1/2$ sublevels. The X-band ^1H ENDOR spectrum of $\text{Mn}(\text{H}_2\text{O})_6^{2+}$ has been well-characterized by Tan et al.²⁶ and sets of ENDOR features have been assigned to different $\Delta m_s = \pm 1$ transitions. It was found that the $A_{\perp} = |A_{\text{iso}} - A_{\text{dip}}|$ features dominated the experimental powder pattern ^1H ENDOR spectra and that the $A_{\parallel} = |A_{\text{iso}} + 2A_{\text{dip}}|$ features appeared as weaker shoulders.^{12,26}

The Q-band ^1H ENDOR spectrum of $\text{Mn}(\text{H}_2\text{O})_6^{2+}$ (Figure 4a), obtained on the first of the six resolved Mn^{2+} EPR lines near $g = 2$, yields features that are centered at the ^1H Larmor frequency of $\nu_n \sim 50$ MHz and are separated by $A_{\text{obs}}(^1\text{H}) = 0.5$ and 2.0 MHz. A set of lower amplitude features at $A_{\text{obs}}(^1\text{H}) = 6.2$ MHz also is observed. The ^1H ENDOR spectrum of the

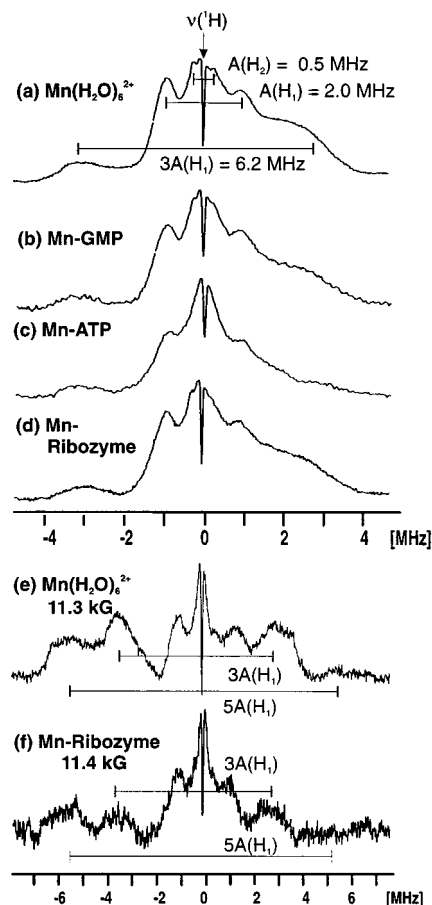


Figure 4. ^1H ENDOR spectra of (a) $\text{Mn}(\text{H}_2\text{O})_6^{2+}$, (b) Mn-GMP, (c) Mn-ATP, (d) Mn-ribozyme, and (e) $\text{Mn}(\text{H}_2\text{O})_6^{2+}$ and (f) Mn-ribozyme at low magnetic field. Spectra a–d were recorded at a field position corresponding to the first of the six $+1/2 \leftrightarrow -1/2$ transitions (~ 240 G below $g = 2$) and show hyperfine couplings at $A_{\text{obs}} = 0.5$, 2.0, and 6.2 MHz. These are assigned to two protons, H_1 with $A_{\perp}(\text{H}_1) \sim 2.0$ MHz ($3 A_{\perp}(\text{H}_1) \sim 6$ MHz) and H_2 with $A_{\perp}(\text{H}_2) = 0.5$ MHz. Spectra e and f were recorded ~ 500 G below that field (11.3 and 11.4 kG, respectively) and show new sets of hyperfine frequencies from H_1 at 11 MHz ($\sim 5 A_{\perp}(\text{H}_1)$). Conditions: (a) 33.97 GHz, 54 scans; (b) 34.05 GHz, 51 scans; (c) 33.77 GHz, 50 scans; (d) 33.83 GHz, 50 scans; (e) 33.98 GHz, 60 scans; (f) 34.01 GHz, 48 scans.

Mn-ribozyme sample (Figure 4d) has features almost identical to those from $\text{Mn}(\text{H}_2\text{O})_6^{2+}$, implying that the Mn^{2+} in the ribozyme contains one or more water molecules in its inner coordination sphere. These ENDOR frequencies can be assigned as the perpendicular components of two populations of hyperfine coupled protons with $A_{\perp}(\text{H}_1) = 2.0$ MHz and $A_{\perp}(\text{H}_2) = 0.5$ MHz.³¹ Each of these are expected to give rise to three sets of $A(^1\text{H})$ frequencies as defined by eqs 3–5 given in Materials and Methods. The lower-amplitude features separated by 6.2 MHz are assigned to $3A_{\perp}(\text{H}_1)$. Similar features for H_2 , expected at $3A(\text{H}_2) = 1.5$ MHz, are not resolved but may be present underneath the broad absorption in that region of the spectrum. ENDOR spectra of the Mn-ribozyme and $\text{Mn}(\text{H}_2\text{O})_6^{2+}$ samples

(30) (a) This EPR simulation, made using Bruker's SimFonia program with $D = -200$ G, is included to illustrate the contributions of $|m_s| > 1/2$ sublevels to the Q-band EPR signal. Others^{12,26,27,30b} have illustrated the D -strain effects at X-band that significantly broaden contributions from the $|m_s| > 1/2$ sublevels at X-band, an effect that is expected to be increased for inhomogeneously broadened systems at higher microwave frequencies. (b) Larsen, R. G.; Halkides, C. J.; Singel, D. J. *J. Chem. Phys.* **1993**, *98*, 6704–6721.

(31) Features assigned to H_1 are separated by values of approximately 2.0, 6.2, and 11.0 MHz. Assuming these values correspond to A_{\perp} , $3A_{\perp}$, and $5A_{\perp}$ respectively gives $A_{\perp}(\text{H}_1) \sim 2.1$ MHz. No obvious features due to A_{\parallel} were observed. We note that the observed A_{\perp} value of 2.1 MHz is less than the 2.4 MHz reported by Tan et al.²⁶ Magnetic fields associated with Q-band microwave frequencies are advantageous in providing resolution between protons and heteronuclei, particularly useful here for ^{31}P measurements, but the increased frequency may also contribute to broader experimental line widths. As discussed by Tan et al.,²⁶ experimental line widths may result in reduced values for the observed hyperfine splittings.

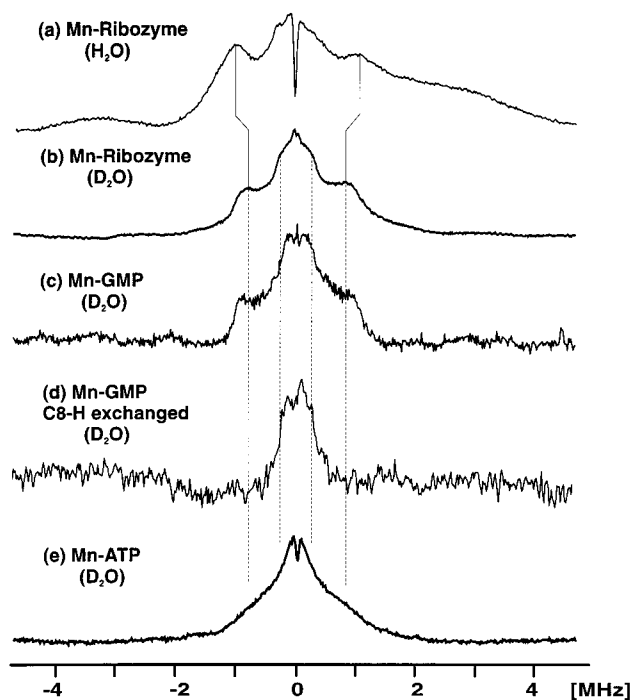


Figure 5. ¹H ENDOR spectra of (a) Mn-ribozyme in aqueous buffer and the deuterium-exchanged samples of (b) Mn-ribozyme, (c) Mn-GMP, (d) Mn-GMP after deuterium exchange of C-8 proton, and (e) Mn-ATP. The spectra were recorded at a field position corresponding to the first of the six $+1/2 \leftrightarrow -1/2$ transitions (~ 240 G below $g = 2$). Conditions: (a) 33.97 GHz, 54 scans; (b) 33.61 GHz, 44 scans; (c) 33.80 GHz, 68 scans; (d) 33.81 GHz, 66 scans; and (e) 33.87 GHz, 42 scans.

taken at a lower magnetic field, a position that is removed from the six-line $\Delta m_s = +1/2 \leftrightarrow -1/2$ EPR features, reveal a decrease in the amplitudes of the $A_{\text{obs}} \sim \leq 2$ MHz ENDOR signals relative to $A_{\text{obs}} \sim 6.2$ MHz, and additional signals appearing at $A_{\text{obs}} \sim 11$ MHz that are assigned to $5A_{\perp}(H_1)$ (Figure 4e,f). The $A_{\text{obs}} = 2.2$ MHz features at this low magnetic field value are close to the expected value of $5A_{\perp}(H_2) = 2.5$ MHz. Taken together, these ENDOR features are assigned to protons from water ligands (H_1) and the second shell of hydration (H_2) about the frozen Mn²⁺ ions,³¹ which by previous analyses have distances of Mn²⁺-H₁ ~ 2.9 Å and Mn²⁺-H₂ ~ 4.4 Å.^{12,26,32,33}

The Mn-GMP and the Mn-ATP complexes in H₂O also show proton ENDOR spectra similar to those observed for Mn-(H₂O)₆²⁺ (Figure 4b,c). The features at $A(H_2) = 0.5$ MHz, assigned above to protons from waters in the second shell of hydration, do not appear to be as resolved in the Mn-ATP complex. This may be due to a more protected environment for the Mn²⁺ ion when chelated by two or more phosphodiester groups and possibly the adenine base (see below) in the ATP complex.

¹H ENDOR: Nonexchangeable Protons. The ¹H ENDOR spectrum of the Mn-ribozyme sample following exchange into deuterated buffer was investigated to identify nonexchangeable protons in close proximity to the Mn²⁺. In Figure 5a and b, the ¹H ENDOR spectrum of a deuterium-exchanged Mn-ribozyme sample, acquired on the first line of the six-line Mn²⁺ EPR signal, is compared with that of a sample in protonated buffer. Deuterium exchange results in a loss of the dominating features

(32) (a) Sivaraja, M.; Stouch, T. R.; Dismukes, G. C. *J. Am. Chem. Soc.* **1992**, *114*, 9600–9603. (b) Zheng, M.; Dismukes, G. C. *J. Phys. Chem. B* **1998**, *102*, 8306–8313.

(33) De Beer, R.; De Boer, W.; Van't Hof, C. A.; van Ormondt, D. *Acta Crystallogr.* **1973**, *B29*, 1473–1480.

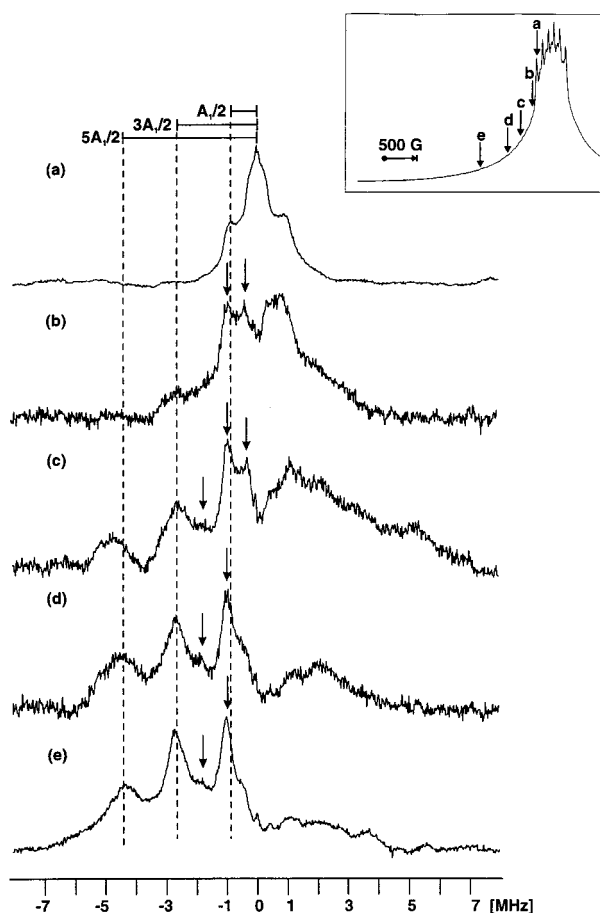


Figure 6. Field dependence of ¹H ENDOR signals from nonexchangeable protons in the hammerhead ribozyme. ENDOR data were obtained at various points on the Mn²⁺ EPR envelope (inset, letters correspond to field locations). Two Mn-¹H coupling patterns are observed from nonexchangeable protons denoted H_{n1} and H_{n2}. The first pattern, indicated by the dashed lines, arises from $A(H_{n1}) = 1.8$ MHz coupled to the $\pm 1/2$, $\pm 3/2$, and $\pm 5/2$ m_s states. The second pattern, indicated by arrows, arises from $A(H_{n2}) = 0.7$ MHz. Conditions: (a) 11 926 G, 33.61 GHz, 44 scans; (b) 11 868 G, 34.08 GHz, 54 scans; (c) 11 671 G, 34.08 GHz, 66 scans; (d) 11 427 G, 34.08 GHz, 68 scans; (e) 11 007 G, 34.08 GHz, 56 scans.

from coordinated water, revealing a spectrum containing two sets of relatively defined features at $A(H_{n1}) = 1.7$ MHz and $A(H_{n2}) = 0.7$ MHz.

To better assign features in the spectra arising from nonexchangeable protons H_{n1} and H_{n2}, ENDOR data were obtained at points on the EPR envelope that would sample different m_s states. At field positions below the $\Delta m_s = +1/2 \leftrightarrow -1/2$ EPR feature (Figure 6b), the amplitudes of some of the ENDOR features decrease and new features grow in. Surprisingly, at positions near the low-field edge of the EPR spectrum (Figure 6d,e), the ENDOR features from nonexchangeable protons became quite sharp, allowing better precision when hyperfine couplings are assigned. The ν_+ partners were not observed in these spectra; such asymmetry in CW Q-band ENDOR has previously been observed.³⁴ Features at $[\nu_n - 2.6]$ MHz and $[\nu_n - 4.3]$ MHz are assigned as the ν_- features corresponding to 3 and 5 times $A(H_{n1}) = 1.7$ MHz (dashed lines in Figure 6). Similarly, signals at $[\nu_n - 1.0]$ MHz and $[\nu_n - 1.7]$ MHz are assigned to the second set of nonexchangeable protons, with $A(H_{n2}) = 0.7$ MHz (arrows in Figure 6). Assuming purely

(34) Telser, J.; Huang, H.; Lee, H.-I.; Adams, M. W. W.; Hoffman, B. M. *J. Am. Chem. Soc.* **1998**, *120*, 861–870.

dipolar coupling and that the observed hyperfine splittings are A_{\perp} , these nonexchangeable protons are at an estimated distance of $r_{n1} \sim 3.6 \text{ \AA}$ and $r_{n2} \sim 4.8 \text{ \AA}$ from the Mn^{2+} ion, respectively.

Proton ENDOR spectra of Mn-GMP and Mn-ATP samples exchanged with D_2O and measured in deuterated buffer show features from nonexchangeable protons with hyperfine couplings similar to the $A(^1\text{H}_{n1}) = 1.7 \text{ MHz}$ observed in the ribozyme (Figure 5c,e). In Mn-GMP, the closest nonexchangeable proton to the N7-coordinated Mn^{2+} would be expected to be the proton at position C8 (C8-H) of the guanine base. Simple molecular modeling of Mn^{2+} complexed with GMP, with a Mn-N7 bond distance of 2.0 \AA , gives a Mn^{2+} -C8-H distance of $\sim 3.4 \text{ \AA}$.³⁵ The guanine C8 proton is exchangeable with mild heating in the presence of D_2O .³⁶ As shown in Figure 5d, this procedure removes the $^1\text{H}_{n1}$ feature from the Mn-GMP ENDOR spectrum, further supporting its assignment as a purine C8 proton in the hammerhead ENDOR spectrum.

³¹P ENDOR. ³¹P ENDOR was employed to investigate the possibility of phosphodiester coordination in the Mn-ribozyme site. Comparative ENDOR data were obtained on Mn-ATP and Mn-GMP as model compounds for Mn-phosphate inner-sphere (direct) or outer-sphere (through water) coordination, respectively. Control samples of Mn^{2+} combined 1:1 with 13-nucleotide (nt) single-stranded DNA and a 13-nt RNA duplex were measured to determine the ³¹P ENDOR signatures from a Mn^{2+} ion interacting with oligonucleotides in a nonspecific manner.

The ³¹P ENDOR spectrum of Mn^{2+} mixed with a 13-nt RNA duplex shows a peak at the ³¹P Larmor frequency ($\nu_n(^{31}\text{P}) \cong 20 \text{ MHz}$), but no other features that would indicate stronger hyperfine coupling between Mn^{2+} and ³¹P (Figure 7a). Similar results were seen in the sample of Mn^{2+} mixed with the 13-nt DNA sequence (not shown). Thus, in the absence of a specific metal binding site, only "distant" ³¹P ENDOR features^{13a} are observed for these Mn^{2+} -nucleic acid samples.

The Mn-GMP crystal structure indicates that Mn^{2+} is coordinated to the N7 of the guanine base and five water molecules and may interact with the 5'-monophosphate in an outer-sphere, through-water manner.²⁸ Consistent with this, the ³¹P ENDOR spectrum of the Mn-GMP complex shows only a single feature centered at the ³¹P Larmor frequency, with a maximum breadth indicating $A(^{31}\text{P}) = 0.9 \text{ MHz}$ (Figure 7b). No other features were observed that would provide evidence for a more strongly coupled ³¹P in this sample.

By contrast with the previous samples, the Mn-ribozyme and Mn-ATP complexes showed ³¹P ENDOR features arising from more strongly coupled ³¹P as previously observed for inner-sphere Mn-phosphate interactions.⁹⁻¹² Solution NMR studies of Mn-ATP both at a 1:1 ratio and in excess ATP report the Mn^{2+} to be directly coordinated to the α , β , and γ phosphate groups of the ATP.^{29a-e} In agreement with the published NMR and previous X-band ENDOR results,¹² the ³¹P ENDOR spectrum of Mn-ATP in a 1:10 ratio (Figure 7c) shows, in addition to the ³¹P Larmor peak, broad hyperfine features in the range of $A(^{31}\text{P}) \sim 3.8\text{--}4.2 \text{ MHz}$ that indicate inner-sphere Mn-phosphate coordination. This range of observed hyperfine couplings is consistent with other published Mn-phosphate inner-sphere coordinated systems examined by ESEEM spectroscopy.⁹⁻¹¹

The ³¹P ENDOR spectrum of the Mn-ribozyme sample exhibits a peak at $\nu_n(^{31}\text{P})$ and broad features split by $A(^{31}\text{P}) \sim$

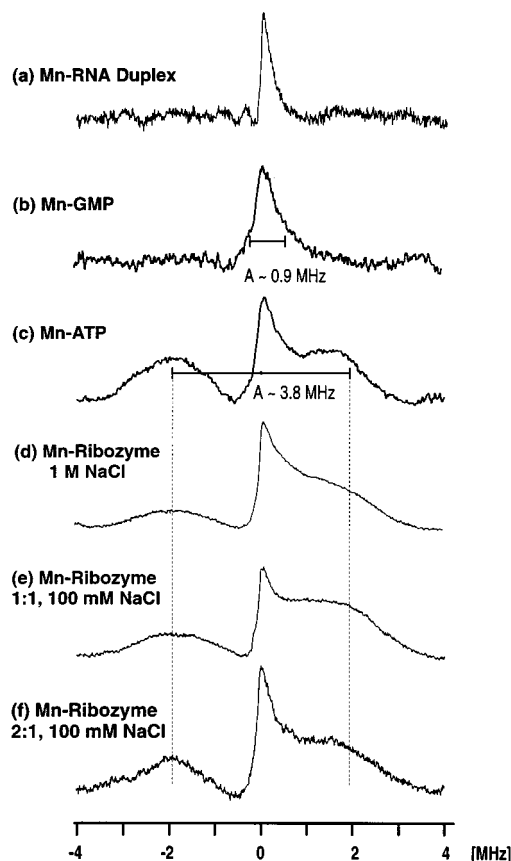


Figure 7. ³¹P ENDOR spectra of (a) Mn-RNA duplex, (b) Mn-GMP, (c) Mn-ATP (d) Mn-ribozyme in 1 M NaCl, (e) Mn-ribozyme in 100 mM NaCl, and (f) 2 Mn-ribozyme in 100 mM NaCl. The spectra were recorded at a field position corresponding to the first of the six $+1/2 \leftrightarrow -1/2$ transitions ($\sim 240 \text{ G}$ below $g = 2$). Conditions: (a) 34.00 GHz, 54 scans; (b) 34.03 GHz, 82 scans; (c) 33.81 GHz, 78 scans 34.00 GHz, 54 scans; (d) 33.83 GHz, 102 scans; (e) 33.98 GHz, 24 scans; (f) 33.98 GHz, 60 scans.

3.8 MHz, similar to but with lower amplitude than those observed in the Mn-ATP sample (Figure 7c,d). From these data, it can be concluded that in 1 M NaCl there is direct coordination between Mn^{2+} and a phosphodiester group in the ribozyme site.

The ribozyme data described above were obtained in a sample containing 1.0 M NaCl, where the ribozyme has a single high-affinity site. In 0.1 M NaCl, the hammerhead ribozyme has four high-affinity sites.¹⁷ ³¹P ENDOR of the Mn-ribozyme samples in 1:1 and 2:1 ratios of Mn^{2+} to ribozyme provide comparative information about the first and second high-affinity Mn^{2+} binding sites occupied in 0.1 M NaCl. The ³¹P ENDOR spectrum of a ribozyme sample prepared in 0.1 M NaCl with 1 equiv of Mn^{2+} is similar to that obtained in 1.0 M NaCl, with features characteristic of an inner-sphere coordinated phosphate having $A_{\text{obs}}(^{31}\text{P}) \sim 3.8 \text{ MHz}$. Addition of a second equivalent of Mn^{2+} yields a similar ³¹P ENDOR spectrum. The relative amplitude of the ³¹P Larmor feature appears to be higher in intensity in the 2:1 Mn^{2+} to ribozyme sample (Figure 7f) as compared to the 1:1 sample (Figure 7e), possibly indicating that the first Mn^{2+} site has an inner-sphere phosphate coordination and the second Mn^{2+} site occupied under these conditions has an outer-sphere phosphate coordination. The line width of the $A(^{31}\text{P}) \sim 3.8 \text{ MHz}$ features appears narrower in the sample with a second Mn^{2+} ion, which could result from a more ordered Mn^{2+} -phosphate geometry upon addition of the second Mn^{2+}

(35) The Mn-N distance modeled using Cerius Molecular Modeling Program with universal force fields.

(36) (a) Taboury, J. A.; Bourtayre, P.; Liquier, J.; Taillandier, E. *Nucleic Acids Res.* **1984**, *12*, 4247-4258. (b) Schweizer, M. P.; Chan, S. I.; Helmkamp, G. K.; Ts'o, P. O. P. *J. Am. Chem. Soc.* **1964**, *86*, 696-700.

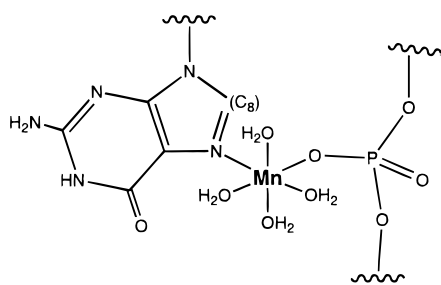


Figure 8. Mn²⁺ ligand environment as predicted by ENDOR studies. The binding site in the hammerhead ribozyme contains a phosphodiester ligand, aqueous ligands, and Mn–guanine N7 coordination as indicated by the nonexchangeable proton assigned to the C8 position. Assignment to guanine is based on results from ESEEM spectroscopic measurements.⁴⁰

ion. It was difficult to obtain ¹H ENDOR on the 2:1 Mn to ribozyme sample, however, possibly due to increased electron spin relaxation caused by the proximity of the second metal ion.

Discussion

The phosphodiester bond cleavage reactions performed by ribozymes may involve several different roles for divalent metal cation(s). Metal-based spectroscopic probes have the potential of providing new methods to observe local environments in RNA molecules and new signals by which metal-dependent activity might be monitored. In these studies, we have examined the local coordination environment of Mn²⁺ in a defined site in the hammerhead ribozyme and compared the results with those of Mn²⁺ in nucleotide model systems. The resulting EPR and ENDOR properties allow the identity and proximity of Mn²⁺ ligands in the hammerhead ribozyme site to be described.

The low-temperature X-band EPR signal of Mn²⁺ in the high-affinity ribozyme site is slightly altered from that of Mn(H₂O)₆²⁺ and reflects a coordination environment that is relatively undistorted from octahedral symmetry. The ¹H and ³¹P ENDOR spectra allow identification of water ligands, inner-sphere phosphate coordination, and nonexchangeable protons that are near to the metal center in the ribozyme. Nonexchangeable proton(s) at ~3.6 Å are assigned to the C8–H of a coordinated purine base. Nonexchangeable proton(s) at ~4.8 Å, which does not correspond to a distance expected for Mn²⁺ coordinated to purines, apparently is(are) from a different sugar or base in the RNA environment.

Interestingly, ¹H ENDOR data also provide evidence for Mn–N7 coordination in the Mn–ATP complex. Early proton NMR data indicated that the Mn²⁺ was directly coordinated to the adenine N7 nitrogen,^{29a} but were contradicted by later data providing evidence for only outer-sphere Mn–N7 coordination via a water molecule.^{29b–d} Sigel and co-workers reported that Mn–ATP complexes exist in a mixture of “closed” and “open” conformations in solution,^{29f} predicting partial population of the Mn–N7 coordinated form.^{29g} This is consistent with the deuterium-exchange ¹H ENDOR data reported here, which support at least partial population of Mn–N7 inner-sphere coordination in Mn–ATP complexes.

Combination of all of the ENDOR data indicates that the coordination environment of the Mn²⁺ in the highest-affinity ribozyme site includes both an inner-sphere phosphate group and purine N7, with the remaining Mn²⁺ coordination sphere filled by water molecules (Figure 8). Only one metal site with these properties has been consistently identified in X-ray

diffraction studies of the hammerhead.^{37,39} This A9–G10.1 site is found in the junction between the conserved core and stem II. Crystals soaked in Mn²⁺ show this site to be populated by Mn²⁺ coordinated directly to a A9 phosphodiester nonbridging oxygen and N7 of the G10.1 base.^{37,39a} Consistent with this assignment, and with the ENDOR data from the nonexchangeable purine C8 proton, we recently have observed ¹⁴N/¹⁵N ESEEM signals in Mn–ribozyme samples that were assigned to direct coordination to guanine.⁴⁰

Although it is approximately 15 Å away from the phosphodiester bond cleavage position in the X-ray crystal structures, the A9/G10.1 site appears to be critical to hammerhead activity.^{23,24} Substitution of the phosphate 5' to A9 with an R_p phosphorothioate inhibits Mg²⁺-dependent cleavage activity, which can be restored by thiophilic Cd²⁺.^{23b,c} Incorporation of an abasic site at this position also inhibits ribozyme activity, which can be recovered by addition of an exogenous guanine base.²⁴ Given its apparent importance in activity, the distance between this site and the active site of the hammerhead in the existing X-ray crystal structures is puzzling. X-ray crystal structures determined in the absence of divalent cations show the same overall hammerhead structure, indicating that population of this site is not required to acquire the folded structure that is observed by X-ray crystallography.^{37,39a} Spectroscopic signals for the A9/G10.1 site under freeze-trapped solution conditions may aid in understanding its role in hammerhead activity.

Of note, all Mn²⁺ EPR signals reported here and in additional studies described below reflect properties only of mononuclear Mn²⁺ sites in the hammerhead. Some proposals for hammerhead and other phosphodiester bond cleavage activity involve two metal ions that form bridged dinuclear metal sites.^{1,2,16c,19} A pair of Mg²⁺ ions in close (4.5 Å) proximity is modeled near the ribozyme active site in the freeze-trapped, pH 8.5 crystal structure of a hammerhead reaction intermediate,³⁷ and molecular dynamics simulations, based on this information, indicated that a μ-bridging OH⁻ would be required to stabilize Mg²⁺ ions at such a distance.³⁸ In the case of Mn²⁺, such a bridge might be expected to give a coupled spin system whose common characteristics include an increased signal breadth and reduced hyperfine splitting of ~45 G.⁵ The addition of 1–4 equiv of Mn²⁺ to the ribozyme in 0.1 M NaCl (pH 7.8) showed increasing amplitude and slight broadening of the mononuclear Mn²⁺ EPR spectra, but no additional features appeared near *g* = 2 or elsewhere in the spectrum. Samples investigated at pH 8.5 (to compare with the intermediate trapped for X-ray crystallography)³⁷ yielded the same result, as did samples using an RNA “substrate” strand with a 2'-OME at the cleavage site to inhibit activity and also a freeze-quenched sample prepared with 10 equiv of Mn²⁺ and an unsubstituted RNA substrate strand (data not shown). Despite an extensive search, at several temperatures with up to 10 equiv of added Mn²⁺ per ribozyme, no additional EPR signals have yet been detected in these samples that would provide evidence for a coupled dinuclear Mn²⁺–Mn²⁺ complex. Thus, if such a bridged dinuclear metal

(37) Scott W. G.; Murray J. B.; Arnold J. R. P.; Stoddard, B. L.; Klug, A. *Science* **1996**, *274*, 2065–2069.

(38) Hermann, T.; Auffinger, P.; Scott, W. G.; Westhof, E. *Nucleic Acids Res.* **1997**, *25*, 3421–3427.

(39) (a) Pley, H. W.; Flaherty, K. M.; McKay, D. B. *Nature* **1994**, *372*, 68–74. (b) Murray, J. B.; Terwey, D. P.; Maloney, L.; Karpeisky, A.; Usman, N.; Beigelman, L.; Scott, W. G. *Cell* **1998**, *92*, 665–673.

(40) Morrissey, S. R.; Horton, T. E.; Grant, C. V.; Hoogstraten, C. G.; Britt, R. D.; DeRose, V. J. *J. Am. Chem. Soc.* **1999**, *39*, 9215–9218. Assignments were based on global ¹⁵N substitution of all G's in the enzyme strand of the hammerhead complex.

site is involved in the hammerhead reaction, it is not populated in the resting-state structure, but must appear in an intermediate that has not yet been trapped in the current experiments.

Few studies have provided detailed structural information about metal sites in RNA under solution conditions.^{41,42} In addition, high ionic strength and variable metal site populations complicate predictions from X-ray crystallography of structured RNA molecules. Thus, there are few comparative studies that allow models from X-ray crystallography to be definitive predictors for metal sites under solution conditions, and so assignment of the Mn²⁺ site examined in this study to the A9/G10.1 site observed by X-ray crystallography remains putative. For example, a recent report by Pardi and co-workers identified a hammerhead ribozyme Mg²⁺ site involving the phosphodiester 5' to A13, an interaction that is not predicted from current crystallographic models.⁴² The ENDOR signals from the Mn-ribozyme complex observed here will allow conclusive site identification using site-specific atom and isotopic substitutions, currently in progress.

Materials and Methods

Hammerhead Sample Preparation. The 34-nt RNA "enzyme" strand was either synthesized by *in vitro* transcription with T7 RNA polymerase⁴³ or purchased (Dharmacon Research, Boulder, CO). "Enzyme" RNA, the 13-nt DNA "substrate" (Integrated DNA Technologies, Coralville, IA), RNA "substrate" (Dharmacon Research), with and without 2'-OMe substitution at the cleavage site, and the complementary 13-nt RNA oligonucleotide (Dharmacon Research) were gel-purified and extensively dialyzed as previously described.¹⁷ Buffer solutions contained 5 mM triethanolamine (TEA) (Sigma), pH 7.8, and 1.0 or 0.1 M NaCl (Alfa Aesar, Puratronic). Oligonucleotide purities were determined by anion-exchange HPLC to be greater than 90%.

Hammerhead complexes were formed by heating 1:1 mixtures of the 34-nt RNA "enzyme" and 13-nt "substrate" oligonucleotides at 90 °C for 3 min, followed by ~20 min incubation at ambient room temperature. Mn²⁺ was added as MnCl₂ (American Analytical, ultrapure grade) following complex formation to yield the desired Mn²⁺ concentration in the sample. In addition, 20% ethylene glycol (v/v) (Aldrich) was added to the samples to serve as a cryoprotectant (see below). The final concentration of Mn²⁺ for ENDOR studies was 1 mM in all cases.

All deuterated samples were prepared in a drybox under a nitrogen atmosphere. TEA/NaCl buffer solutions were prepared in 99.9% D₂O (Cambridge Laboratories), pD = 7.8, and ethylene-*d*₆ glycol obtained from Aldrich (99 atom % D). RNA and DNA oligonucleotides were deuterium-exchanged following precipitation by resuspending the oligonucleotide pellet in 250 μL of D₂O. Following incubation, the sample was lyophilized and the procedure repeated before suspending the sample in the deuterated buffer solution.

Mn-Nucleotide Samples. GMP and ATP (Pharmacia, disodium salt) complexes with Mn²⁺ were 10 mM nucleotide/1 mM Mn²⁺ in TEA buffer/1 M NaCl/20% ethylene glycol. Deuterated samples were prepared by direct suspension into the deuterated buffer/ethylene glycol solutions. Deuterium exchange of the guanine C8 proton was accomplished by incubating a 10 μM sample of GMP (disodium salt) in D₂O at 80 °C for 5 h.³⁶ Following incubation, the exchanged GMP sample was prepared under a dry nitrogen atmosphere as described above.

Activity Measurements. Ribozyme activities were measured using 5' ³²P-labeled 13-nt RNA "substrate" and 34-nt RNA "enzyme" strand (5'-triphosphate) as previously described.¹⁷

Cryoprotectant. Several cryoprotectants were evaluated for low-temperature studies of the hammerhead ribozyme. Criteria included the following: (1) metal binding assays using room-temperature EPR to monitor affinities of the "tight" Mn²⁺ sites; (2) activity measurements in 10 mM Mn²⁺; (3) observation of a ¹H ENDOR signal. Feig et al. reported that cryoprotectants consisting of 40% (v/v) methanol, 20% (v/v) glycerol, and 30% (v/v) ethylene glycol were maximum limits to maintain 80% of control hammerhead ribozyme activities.⁴⁴ For the spectroscopic studies reported here, it was found that methanol and sucrose were insufficient cryoprotectants for EPR/ENDOR spectroscopy, and glycerol interfered with Mn²⁺ binding to the ribozyme at low Mn²⁺ concentrations. Ethylene glycol (20%, v/v), however, was found to give Mn²⁺ binding and activity levels identical to those in the absence of any cryoprotectant and therefore was used in all low-temperature EPR and ENDOR studies.

EPR and ENDOR Experiments. Room-temperature and 10 K X-band EPR data were obtained on a Bruker ESP-300 spectrometer equipped with a TE₁₀₂ cavity. Q-band (34 GHz) EPR and ENDOR experiments were performed on a locally constructed continuous-wave spectrometer consisting of a Varian E-110 microwave bridge, Bruker ESP-200 console, and ER-073 magnet interfaced using LabView-based hardware and software.⁴⁵ The TE₀₁₁ cavity, constructed as described by Sienkiewicz et al.,⁴⁶ has a movable end plate for frequency tuning. Radio frequency (PTS 160 frequency generator and ENI 3200L broadband power amplifier) and magnetic field modulation were introduced into the resonant cavity by two sets of two single-turn coils (connected in series) formed by copper-coated silver wire (23 gauge, MWS Wire Industries) and oriented perpendicular to each other. The cavity is immersed in a Janis 7.5 CNDT-SVT liquid helium immersion cryostat, providing operating temperatures of 2.0–2.2 K.

ENDOR spectroscopy was performed by monitoring the intensity of the low-temperature EPR signal detected in dispersion under conditions of rapid passage with 100 kHz field modulation^{13a,b,47,48} as a function of applied radio frequency. Typical acquisition parameters were as follows: 1–10 mW microwave power, 0.5 G ptp 100 kHz field modulation, 20 W applied rf power, 2.0–2.2 K, and 0.25–0.5 MHz/s rf sweep rate. The samples, prepared as described above, were placed in 2.0 i.d. × 2.4 o.d. quartz capillary tubes (Wilmad Glass) and glassed in liquid nitrogen prior to immersion in the cryostat. The sample volume used in the ENDOR experiments ranged from 60 to 75 μL. Data processing was performed using the Bruker WINEPR program, version 2.11. Acquired ENDOR spectra are inverted, and a smoothly varying baseline is subtracted for presentation.

Mn²⁺ EPR spectra were simulated using SimFonia (Bruker). This program is based on perturbation theory and calculates allowed transitions for the situation in which the electronic Zeeman interaction is the dominating interaction. The program does not include zfs-dependent line broadening as has been simulated by others.^{12,26,30b}

ENDOR Frequencies. The first-order ENDOR frequencies⁴⁹ (ν_{\pm}) for a nuclear spin of 1/2 hyperfine coupled to a paramagnetic center with m_s spin states are defined as

$$\nu_{\pm} = |\nu_n \pm m_s A| \quad (1)$$

where ν_n is the Larmor frequency of the coupled nuclei and A is the hyperfine coupling constant. Specifically for Mn²⁺, eq 1 becomes

$$\nu_{\pm} = |\nu_n \pm A/2| \quad (2)$$

$$\nu_{\pm} = |\nu_n \pm 3A/2| \quad (3)$$

(44) Feig, A. L.; Ammons, G. E.; Uhlenbeck, O. C. *RNA* **1998**, *4*, 1251–1258.

(45) Acquisition program written by Dr. Tomasz Wasowicz.
(46) Sienkiewicz, A.; Smith, B. G.; Veselov, A.; Scholes, C. P. *Rev. Sci. Instrum.* **1996**, *67*, 2134–2138.

(47) Feher, G. *Phys. Rev.* **1956**, *103*, 834–835.
(48) Werst, M. M.; Davoust, C. E.; Hoffman, B. M. *J. Am. Chem. Soc.* **1991**, *113*, 1533.

(49) Abragam, A.; Bleaney, B. *Electron Paramagnetic Resonance of Transition Ions*; Dover: New York, 1986.

(41) (a) Kieft, J. S.; Tinoco, I., Jr. *Structure* **1997**, *5*, 713–721. (b) Gonzalez, R. L., Jr.; Tinoco, I., Jr. *J. Mol. Biol.* **1999**, *289*, 1267–1282 (c) Allain, F. H.; Varani, G. *Nucleic Acids Res.* **1995**, *23*, 341–350.

(42) Hansen, M. R.; Simorre, J.-P.; Hanson, P.; Mokler, V.; Bellon, L.; Beigelman, L.; Pardi, A. *RNA* **1999**, *5*, 1099–1104.

(43) Milligan, J. F.; Uhlenbeck, O. C. *Methods Enzymol.* **1989**, *180*, 51–62.

$$\nu_{\pm} = |\nu_n \pm 5A/2| \quad (4)$$

The resulting ENDOR spectrum taken at a field where all Δm_s transitions contribute will therefore consist of a superposition of the frequencies described by eqs 2–4. For the case where $\nu_n > A$, appropriate for the ¹H and ³¹P data presented here, the set of ENDOR features will be centered at ν_n and split by A . For an axially symmetric hyperfine interaction, powder patterns will be defined by

$$A_{\perp} = |A_{\text{iso}} - A_{\text{dip}}| \quad (5)$$

$$A_{\parallel} = |A_{\text{iso}} + 2A_{\text{dip}}| \quad (6)$$

where the higher-intensity features due to A_{\perp} have been found to dominate the Mn²⁺ ENDOR spectrum in previous studies.^{12,26,32} Assignment of A_{dip} allows estimation of distances using the point–dipole approximation of eq 7, where r is the distance between the metal

$$A_{\text{dip}} = (1/r^3)g_n\beta_n g_e\beta_e (3 \cos^2\theta - 1) \quad (7)$$

ion and the observed nuclear spin, θ is the angle between the vector connecting the two spins and the external magnetic field, g_e and g_n are the electron and nuclear g value, and β_e and β_n are the Bohr and nuclear magneton, respectively.

Acknowledgment. Dr. Tomasz Wasowicz made critical contributions in construction of the Q-band ENDOR spectrometer. This work was supported by the NSF (CAREER award to VJD, CHE-8912763 for Texas A&M EPR facilities), the NIH (GM58096), the Robert A. Welch Foundation, and the Texas Higher Education Coordinating Board Advanced Research Program. V.J.D. is a Cottrell Scholar of the Research Corporation.

JA992989Z